Ultrasonic Devulcanization of Rubber Vulcanizates. I. Process Model

A. I. ISAYEV,* S. P. YUSHANOV, and J. CHEN

Institute of Polymer Engineering, University of Akron, Akron, Ohio 44325-0301

SYNOPSIS

Tire and rubber waste recycling is an important issue facing the rubber industry. In addressing this issue, the present article describes the first attempt to formulate a model and to simulate a novel continuous ultrasonic devulcanization process. The proposed model is based upon a mechanism of rubber network breakup caused by cavitation, which is created by high-intensity ultrasonic waves in the presence of pressure and heat. Dynamics of bubble behavior is described by the Notlingk–Neppiras equation with incorporation of an additional term based upon elastic strain-energy potential. Acoustic pressure arising in the ultrasonic field is related to void formation. Their concentration is calculated based upon nucleation and growth of gas bubbles in crosslinked elastomers under negative driving pressure. The breakup of a three-dimensional network in crosslinked rubbers is combined with flow modeling. The viscosity function required for this modeling is based upon a power-law model which includes temperature, shear rate, and gel fraction dependence. © 1996 John Wiley & Sons, Inc.

INTRODUCTION

During the last decade, Isayev and co-workers[1-3] carried out extensive studies in an attempt to develop a polymer processing technology which utilizes high-power ultrasonics. It was shown that during extrusion high-intensity ultrasonic waves affect the die characteristics by reducing the pressure and die swell and postpone melt fracture. The ultrasonic waves can also breakdown the molecular chains which permanently reduce the viscosity of the original polymer melt. The breakdown of molecular chains occurs not only in polymer melts but also in polymer solutions. Degradation of polymer solutions has a long history.[4-6] There is now overwhelming evidence that degradation in polymer solutions occurs as a result of the cavitation process associated with the stresses generated by the ultrasonic waves and their rate of change. The effect of cavitation is due to the presence of voids or density fluctuation in a liquid. The mechanism of the ultrasonic effect on fluids was extensively studied by Suslick and co-workers.[7,8] Acoustic cavitation is also observed in polymer melts.[9] It has also been found that high-intensity ultrasonics imposed during foam formation improve the uniformity, reduce the size of the cell structure, and enhance the mechanical properties of the foam.[10]

Recently, it was discovered that ultrasonic waves of certain levels, in the presence of pressure and heat, rapidly breakup the three-dimensional network in vulcanized rubbers.[11,12] The devulcanized rubber becomes soft. It can be reprocessed, shaped, and revulcanized in much the same way as a virgin rubber.[13] The process of ultrasonic devulcanization is very fast and occurs on the order of a second or less. The latter allowed us to develop a continuous process of devulcanization. References 13 and 14 also described some recent preliminary experiments and efforts to understand a possible mechanism of the devulcanization and attempt to scale up the process. In particular, the performed measurements indicate that the rubbers are partially devulcanized and the devulcanization process is accompanied by some degradation. In addition, the preliminary results of the modeling of the process of devulcanization were reported in Ref. 15, where a simple model was formulated and simulation results were compared with

* To whom correspondence should be addressed.

Journal of Applied Polymer Science, Vol. 59, 803–813 (1996)
 CCC 0021-8995/96/050803-11

experiments. Furthermore, a review of alternative methods of devulcanization including chemical, thermomechanical, and microwave techniques was presented in recent papers by Warner[16] and Isayev et al.[13]

The present study describes the further development of a theoretical model proposed in Ref. 15 for the devulcanization process. The present modification of the process model includes the improved treatment of the kinetics of void formation and considers the interaction among acoustic pressure amplitude, ambient pressure, void fraction in rubber, and parameters of ultrasonic waves. A simulation and comparison between predicted and experimental data are to be presented in the Part II of this study.

THEORETICAL MODELING

Theoretical modeling of the devulcanization process includes two main aspects: (1) on a microlevel, network degradation in ultrasonic fields, and (2) on a macrolevel, material behavior (temperature, pressure, velocity and shear rate) during flow in the devulcanization process. Evidently, the temperature, pressure, etc., affect the rate of the network degradation and vice versa. These two problems are inherently coupled, and they cannot be solved separately. In addition, there are many particular subproblems such as molecular structure and structural behavior of the network which have to be studied theoretically in more detail. Thus, some simplifying assumptions should be made to handle this task. The proposed model inevitably includes fitting parameters which are to be specified based on comparison between theoretical modeling and experimental data. The number of the fitting parameters are kept to a minimum.

Devulcanization Modeling

In formulating the devulcanization model, the following assumptions are made: (1) The breakup of the network chains and crosslinks are independent processes; (2) the overall rate of molecular breakup is inversely proportional to the relative strength of the bond and proportional to the number of locally overstressed molecular bonds; (3) the rate of devulcanization is governed by an average residence time (this assumption leads to a uniform rate of devulcanization at any particular cross section); and (4) cavitation is a dominant mechanism governing the devulcanization process and collapsing cavities are considered to be noninteractive. Experimental evidence indicating the presence of cavitation in the devulcanization process is given in Part II of this study.

Based on assumptions 1–3, the rate of breakup for various bonds can be written as

$$-\frac{\partial N_i(t)}{\partial t} = k_1 N_{ia}(t)\frac{E_0}{E_i}; \quad N_i(0) = N_{i0} \qquad (1)$$

where $N_i(t)$ is the number of the molecular bonds present in the system at an average residence time t, with N_{i0} being their number at some initial time; N_{ia}, the current number of "active" molecular bonds which are subjected to a local overstressing; E_i, the bond strength; E_0, the reference strength (carbon–carbon bond strength can be chosen as E_0, i.e.: $E_0 = E_C$); and k_1, a rate constant. In eq. (1), the subscript i denotes the specific type of the molecular bonds under consideration: $i = C$ refers to the C—C bonds of the main chain, $i = \nu_k$ refers to the crosslinks of k-th type (e.g., $i = \nu_1$ for monosulfidic C—S—C, and $i = \nu_x$ for polysulfidic C—$\underbrace{S\cdots S}_{x}$—C crosslinks).

Based on assumption 4, the number of "active" bonds per unit volume can be expressed as

$$N_{ia} = \Delta V_a N_i N_b \qquad (2)$$

where ΔV_a is the "active" volume around a single collapsing bubble (Fig. 1), and N_b, the concentration of the collapsing bubbles. The product of $\Delta V_a N_i$ is the fraction of the total existing bonds which are affected by local overstressing around a single collapsing bubble. In turn, the "active" volume ΔV_a is the volume of the spherical shell with inner radius

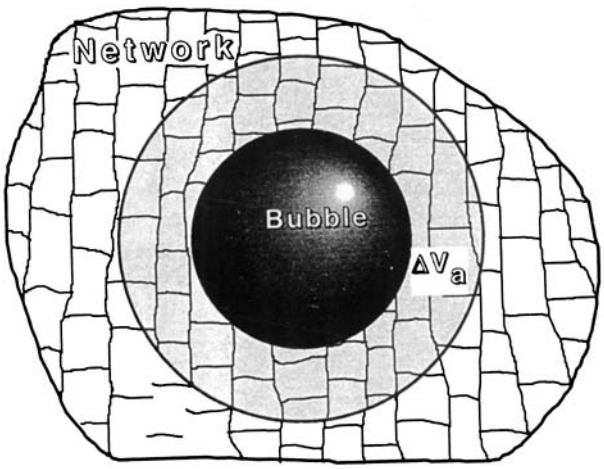

Figure 1 Schematic of the overstressed network fragment around the collapsing bubble.

R_{max} and thickness ΔL_a, where R_{max} is the bubble radius just before collapsing. The parts of the molecular chains located near the collapsing bubble are subjected to the highest tensile forces which are supposed to be high enough to breakup the molecular bonds. The acting forces are decreasing with increasing distance from the bubble wall and above some distance ΔL_a are not sufficient to breakup the molecular bonds. It is assumed that ΔL_a is of the order of the Kuhn's segment[17] length with the molecular chain considered to be rigid. To estimate the value of the ΔL_a more precisely, one needs to consider the problem of the dynamic network deformation and stress distribution around the collapsing bubble. This problem is out of our scope now, and here we will treat ΔL_a as a model parameter satisfying condition $\Delta L_a \ll R_{max}$. Hence,

$$\Delta V_a = \frac{4}{3}\pi[(R_{max} + \Delta L_a)^3 - R_{max}^3] \approx 4\pi R_{max}^2 \Delta L_a \quad (3)$$

The magnitude of R_{max} is determined from the simulation of the cavitation process in crosslinked rubber. It is a function of the intensity of the ultrasonic waves, the current hydrostatic pressure, the frequency and amplitude of the ultrasonic waves, and the elastic characteristics of the material. A description of the modeling of the cavitation process is presented in the next section.

Integration of eq. (1) and making use of eqs. (2) and (3) leads to

$$N_i(t) = N_i(0)\exp\left[-4\pi K \frac{E_C}{E_i} \times \int_0^t R_{max}^2(t) N_b(t)\, dt\right] \quad (4)$$

where $K = k_1 \Delta L_a$ is a constant. In eq. (4), the values R_{max} and N_b are time-dependent since they are the functions of pressure which, in turn, varies with flow along the die length. The constant K is fitting parameter which is to be specified from comparison of the theoretical and experimental results on the gel fraction of the material after devulcanization.

Now, one needs to specify the values of $N_i(0)$ in eq. (4). Suppose that the network was produced from originally "infinite" linear molecules by the addition of different kinds of crosslinks: $\nu = \sum \nu_k$, where ν_k is the number of moles of the k-th crosslinks in a unit volume, and ν, the total number of moles of various crosslinks in a unit volume. The number of moles of the "ideal" network chains (the main chain segments between two subsequent crosslinks) in a unit volume is equal[18] to $n = 2\nu$. Hence, the number of the network chains, N_C, and the number of k-th crosslinks, N_{ν_k}, in a unit volume are given by

$$N_C(0) = nN_A = \frac{\rho_0 N_A}{M_c}, \quad N_{\nu_k}(0) = \nu_k N_A \quad (5)$$

where ρ_0 is the material density; M_c, the molecular weight of the initial network chain; and N_A, Avogadro's number. Relations given by eq. (5) are the initial conditions for the calculation of the kinetics of network chains and crosslinks degradation.

With an increasing amount of main chain and crosslink scissions, the gel fraction decreases. Modeling the gel fraction in relation to the number of broken main chains and crosslinks is a complex problem and needs special consideration. One can use, e.g., the Monte Carlo technique to solve this problem. However, it is clear that if there are no broken crosslinks the network gel fraction is equal to one. If all crosslinks are broken, the gel fraction is equal to zero. As a first approximation satisfying these conditions, one can use the following equation to estimate the network gel fraction $\xi(t)$ at time t:

$$\xi(t) = \xi_0 - \frac{2[N_\nu(0) - N_\nu(t)]}{N_C(0)} \quad (6)$$

where ξ_0 is a gel fraction of the original material, and $N_\nu(t)$, the material crosslink density at time t:

$$N_\nu(t) = \sum_k N_{\nu_k}(t) \quad (7)$$

Cavitation Modeling

Let us consider a spherical bubble contained in a large body of an incompressible polymer. Initially, at time $t = 0$, the system is at rest with a bubble radius R_0 and uniform ambient pressure P_0. The equation for the spherically symmetric motion for a gas bubble, in which there is no gas condensation or evaporation, can be reduced to[19]

$$R\ddot{R} + \frac{3}{2}\dot{R}^2 = \frac{P_i(t) - P_\infty(t)}{\rho_0} \quad (8)$$

where $r = R(t)$ is the radial position of the bubble–polymer interface, with P_i and P_∞ denoting the pressure in the polymer at $r = R(t)$ and $r = \infty$,

respectively. The dots denote derivatives with respect to t. Equation (8) is a linear momentum conservation principle. It states that the media outside the bubble wall accelerates in response to pressure driving forces $(P_i - P_\infty)$.

Based on the force balance at the bubble–polymer interface in the cavity, the term P_i in eq. (8) can be expressed in terms of surface tension, σ, and the radial stress, τ_{rr},

$$P_g = P_i + \tau_{rr,i} + \frac{2\sigma}{R} \tag{9}$$

where g refers to any gas which may be present in the cavity, and i, to the polymer–gas interface. Assuming adiabatic changes, the gas pressure is expressed as[20]

$$P_g = \left(P_0 + \frac{2\sigma}{R_0}\right)\left(\frac{R_0}{R}\right)^{3\gamma} \tag{10}$$

where γ is the ratio of the specific heats of the gas.

The term $\tau_{rr,i}$ takes into account the elastic response of polymer due to the bubble motion. This response can be estimated by means of the theory of large deformations assuming a particular form of the stored-energy function, W, for the rubber. In the present case, the value of $\tau_{rr,i}$ is calculated based on the deformation caused by the inflation of a thick-walled spherical shell.[21] For a shell with an infinitely thick wall (e.g., for a rubber block containing a small spherical cavity, Fig. 2), the relation between inflation pressure, P_m, and extension ratio, $\lambda = (R/R_0)$, of the circumference of the inner surface takes the form[22]

$$P_m(\lambda) = W_1\left(5 - \frac{4}{\lambda} - \frac{1}{\lambda^4}\right) + \frac{W_2}{3}\left[\ln\left(\frac{3\lambda^6}{2+\lambda^6}\right) + 2\sqrt{2}\left\{\tan^{-1}\sqrt{2} - \tan^{-1}\left(\frac{\sqrt{2}}{\lambda^3}\right)\right\}\right] \tag{11}$$

In deriving this equation, it is assumed that rubber obeys a logarithmic form for the stored-energy function[23]:

$$W = W_1(I_1 - 3) + W_2\ln\left(\tfrac{1}{3}I_2\right) \tag{12}$$

In eq. (12), I_1 and I_2 are the strain invariants and W_1 and W_2 are constants.

For the cavity in equilibrium state, $\tau_{rr,i} = P_m$. Hence, the interfacial pressure is given by

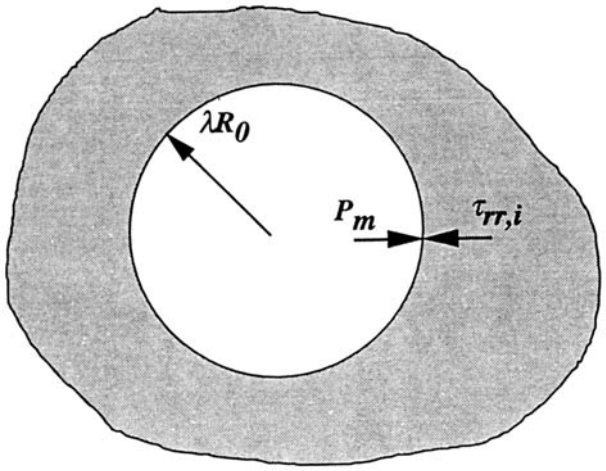

Figure 2 Inflation of a cavity contained in a large body.

$$P_i = \left(P_0 + \frac{2\sigma}{R_0}\right)\left(\frac{R_0}{R}\right)^{3\gamma} - \frac{2\sigma}{R} - P_m\left(\frac{R}{R_0}\right) \tag{13}$$

When a cavity is set into motion by sound field, both the pressure at the interface and at infinity will be functions of time

$$P_\infty(t) = P_0 - P_A\sin 2\pi ft \tag{14}$$

where P_0 is the steady-state ambient pressure; f, the ultrasonic frequency; and P_A, the amplitude of the driving ultrasound pressure. A sign convention is used so that as the time initially increases the pressure falls and the radius of the bubble increases.

Putting (13) and (14) in eq. (8) leads to the equation that governs the evolution of the bubble:

$$R\ddot{R} + \frac{3}{2}\dot{R}^2 = \frac{1}{\rho_0}\left[\left(P_0 + \frac{2\sigma}{R_0}\right)\left(\frac{R_0}{R}\right)^{3\gamma} - \frac{2\sigma}{R} - (P_0 - P_A\sin 2\pi ft) - P_m\left(\frac{R}{R_0}\right)\right] \tag{15}$$

under the initial conditions $R(0) = R_0$, $\dot{R}(0) = 0$ with P_m to be calculated by (11), and P_A is defined by the media acoustic response as described in the next section. It should be noted that if $P_m \equiv 0$, eq. (15) reduces to well-known Notlingk–Neppiras dynamic bubble equation.[24,25]

Acoustic Pressure and Void Fraction

The ultrasound pressure amplitude is calculated by the formula[26]

$$P_A = 2\pi\rho_0 c_s f A \tag{16}$$

where c_s is the velocity of the sound in polymer, and A, the ultrasound amplitude. The presence of small gas bubbles in a polymer (bubbly polymer) produces acoustic properties differing a great deal from those of pure polymer, even if the gas concentration is small. This is because the compressibility of the mixture is substantially altered, reducing the speed of sound. The problem of the sonic speed in a bubbly media has been studied extensively in the literature.[27-30] A homogeneous polymer mixture of bubbles with equal radii R_0 can be characterized by the void fraction φ which is the volume occupied by the bubble in a unit volume of the mixture. If N_b is the number of bubbles per unit volume, the volume fraction is

$$\varphi = \frac{4}{3}\pi R_0^3 N_b \tag{17}$$

Nucleation and growth of gas bubbles in cross-linked elastomers were studied experimentally by Gent and Tompkins.[31] It was found that the number of primary bubbles per unit volume depends exponentially on a negative driving pressure. Below some value of pressure, P_c, no visible bubbles formed. Taking into account this experimental result, one can write for the case of negative driving pressure $(P_A - P_0)$:

$$N_b = N_0 \exp[\beta(P_A - P_0)]H(P_A - P_0) \tag{18}$$

where N_0 and β are constants characterizing initial bubble concentration and sensitivity of bubble formation in polymer due to pressure variation. These constants depend on the conditions of bubble formation and material properties. In eq. (18), $H(\cdot)$ is the Heviside function (unit step function).

The sound velocity in the bubbly media is calculated as[32]

$$c_s = \frac{1}{\sqrt{c_0^{-2}(1-\varphi)^2 + c_M^{-2}}} \approx \frac{c_0 c_M}{\sqrt{c_0^2 + c_M^2}} \tag{19}$$

where c_0 is the sound velocity in polymer without bubbles, and c_M, the velocity defined by Mallock's formula

$$c_M^2 = \frac{\gamma P_0}{\rho_0 \varphi} \tag{20}$$

For the small voids concentration, $\varphi \ll 1$, velocity (20) is consistent with the well-known result by van Wijngaarden[28]:

$$c_W^2 = \frac{\gamma P_0}{\rho_0 \varphi(1-\varphi)}$$

After substitution (19) into (16) with account of (17), (18), and (20), eq. (16) reduces to the following transcendental equation with respect to acoustic pressure amplitude:

$$P_A = \frac{2\pi\rho_0 c_0 f A}{\sqrt{1 + \frac{4}{3}\pi R_0^3 \frac{c_0^2 \rho_0}{\gamma P_0} N_0 \times \exp[\beta(P_A - P_0)]H(P_A - P_0)}} \tag{21}$$

Solving eq. (21) with respect to P_A, the number of bubbles, N_b, and their volume fraction φ are calculated by (18) and (17), respectively.

Figure 3 presents plots of the acoustic pressure amplitude vs. the ambient pressure as obtained from numerical solution of the eq. (21). Results are shown for adiabatic ($\gamma = 1.4$) bubble behavior with their average radius $R_0 = 25$ μm. The sound velocity c_0 is taken to be 2000 m/s. The parameter $N_0 = 4.7 \cdot 10^3$ m^{-3} is adopted from experimental data presented by Gent and Tompkins.[31] They pointed out that the value of N_0 is not sensitive to temperature variation, whereas the rate of bubbles formation (which is proportional to parameter β) increased markedly at higher temperatures. Due to this reason, parameter N_0 is kept constant, while parameter β in eqs. (18) is varied. The dependence of the acoustic pressure amplitude on the ambient pressure is highly nonlinear. Bubbles start nucleating if the driving pressure $(P_A - P_0)$ exceeds some value P_c. The presence of

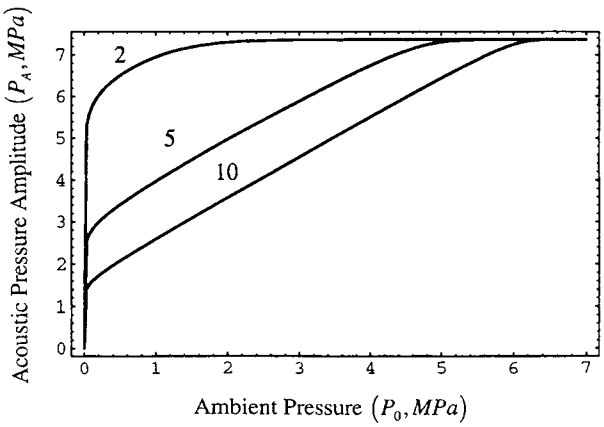

Figure 3 Dependence of the acoustic pressure amplitude on the ambient pressure at various values of β, MPa^{-1}. f = 20 kHz, A = 31.5 μm, and R_0 = 25 μm.

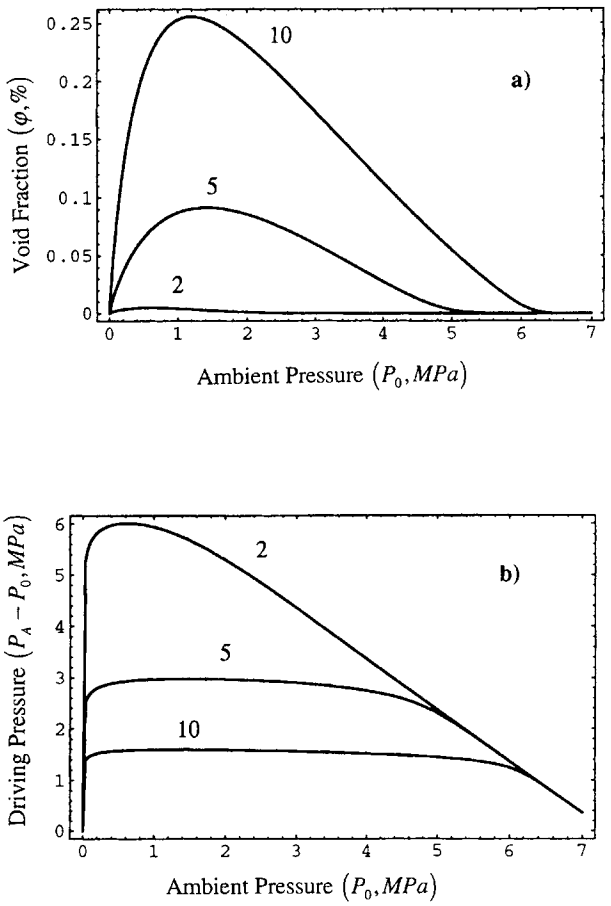

Figure 4 Dependencies of the (a) void fraction and (b) driving pressure on the ambient pressure at various values of β, MPa^{-1}. f = 20 kHz, A = 31.5 μm, and R_0 = 25 μm.

voids reduces the sound velocity in bubbly media and, consequently, according to eq. (16), reduces the acoustic pressure amplitude. An increase in ambient pressure results in suppressing the voids formation. This leads to the increasing in acoustic pressure amplitude until the ambient pressure reaches some value P_0^* which is high enough to suppress completely the nucleation of bubbles. Further increase in ambient pressure does not change the value of acoustic pressure amplitude which reaches its upper limit P_A^* defined by the sound velocity in the polymer without the presence of voids: $P_A^* = 2\pi\rho_0 c_0 f A$. The value P_0^* as well as the slope of acoustic pressure amplitude dependence on ambient pressure are functions of parameter β as illustrated in Figure 3.

The dependence of void fraction on ambient pressure has a pronounced maximum [Fig. 4(a)]. This maximum is attributed to the maximum of the driving pressure, $(P_A - P_0)$, depicted in Figure 4(b). The initial increase of the void fraction at low values of ambient pressures is attributed to the increase in acoustic pressure amplitude. However, further increase in ambient pressure leads to a decrease in $(P_A - P_0)$ and therefore lowers the number of voids formed.

Maximum Cavitation Bubble Radius

The maximum radius of the collapsing bubble is an important parameter affecting the rate of network degradation. According to eq. (4), the rate of breakup of bonds is proportional to $R_{\max}^2$. The value $R_{\max}$ is determined from the numerical solution of the dynamic bubble eq. (15) for media elastic response P_m defined by eq. (11) and acoustic pressure P_A being calculated from eq. (21).

The dependencies of the relative radius R/R_0 on the dimensionless time t/t_p are shown in Figure 5 with $t_p = (1/f)$ being the ultrasound wave period. The parameter of the illustrated family of curves is the ambient pressure P_0 (in MPa). For a given value

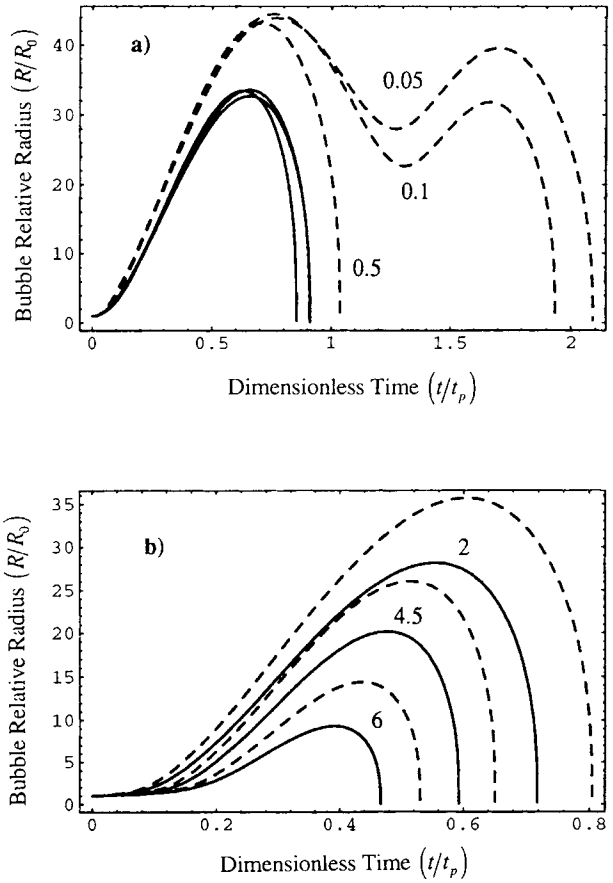

Figure 5 Bubble radius–time curves for different ambient pressures (solid lines) for media elastic response and (dashed lines) for the Notlingk–Neppiras model. f = 20 kHz; A = 31.5 μm; R_0 = 25 μm; β = 5 MPa^{-1}.

of P_0, the value of acoustic pressure amplitude is determined uniquely according to Figure 3. The parameters γ and σ are adopted as $\gamma = 1.4$ and $\sigma = 0.036$ N/m. The constants W_1 and W_2 of the stored-energy function (12) were determined from the experimental stress–strain curve for SBR. This data along with the fitted curve are given in Figure 6. The curve corresponds to eq. (12) with $W_1 = 0.12$ MPa and $W_2 = 0.085$ MPa.

The character of the radius–time curve depends on the value of the ratio P_A/P_0 provided that all other parameters are the same. If the acoustic pressure amplitude is much larger than the ambient pressure, a cavity will expand to many times its original size. As seen from Figure 3, the higher values of P_0 lead to the lower ratios of P_A/P_0 due to saturation of the acoustic pressure amplitude at high ambient pressures. Furthermore, if the acoustic pressure amplitude is equal to the ambient pressure, a cavity will not expand since there is no driving force to its expansion ($P_A - P_0 = 0$). Therefore, the closer to unity the ratio P_A/P_0 is, the lower is the value of R_{max}/R_0, as shown in Figure 5(a) and (b). A

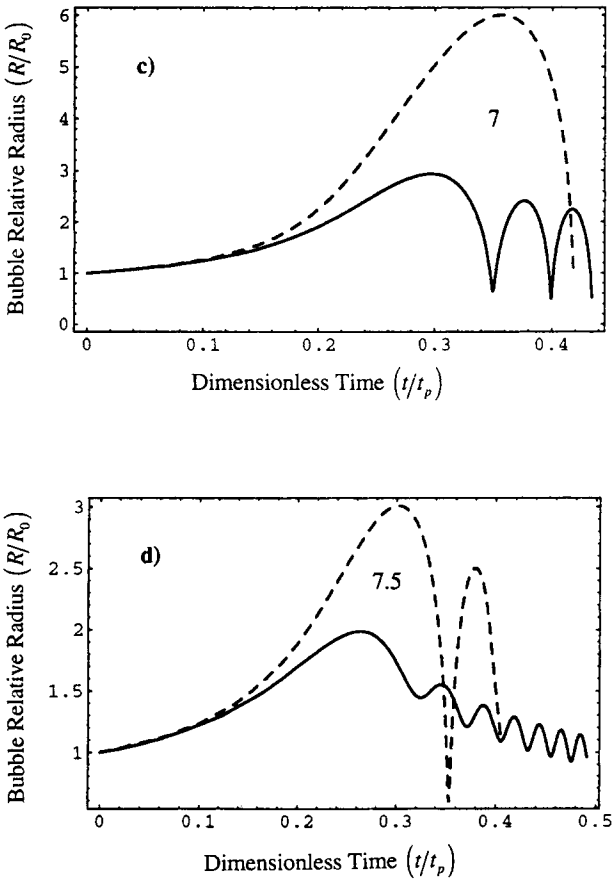

Figure 5 *(Continued from the previous page)*

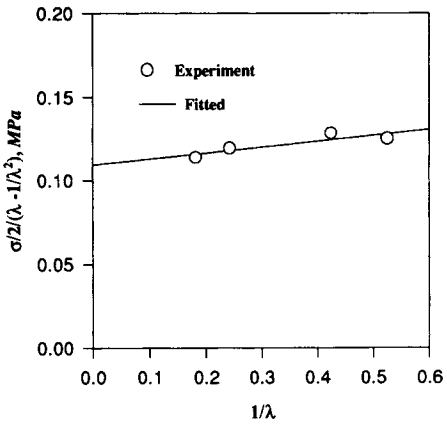

Figure 6 Mooney–Rivlin plot of samples of the virgin SBR vulcanizate at the elongational speed of 0.42 mm/s.

larger value of R_{max}/R_0 causes a more violent collapse. The bubble response is highly affected by the ambient pressure. At high ambient pressure when the ratio P_A/P_0 approaches 1, the bubble becomes involved in nonlinear oscillations, as indicated in Figure 5(c) and (d). Although with increase in ambient pressure the amplitude of the acoustic pressure increases, the driving pressure is not high enough to collapse the bubble as a transient cavity. The first collapse will occur near the peak of acoustic pressure. On collapse, the bubble may not disintegrate as it would if it were transient, but may oscillate for the remainder of the ultrasound cycle at its own natural frequency.

Figure 5 also illustrates the media elastic effect on the dynamics of a bubble cavitation. The solutions of eq. (15) with neglecting of the media elastic response ($P_m = 0$) is plotted in Figure 5 by dashed lines. The main conclusion is that media elastic response reduces the maximum cavitation bubble radius as well as the collapse time. This effect is obvious since in eq. (15) the elastic term P_m has the same influence on bubble dynamics as does the ambient pressure P_0. At low ambient pressures, the bubble according to the Notlingk–Neppiras model shows characteristic dynamic behavior; namely, during the rarefied ultrasound pressure phase, a point is reached where the bubble has grown so large that it has no time to collapse completely before the end of pressure cycle. It will collapse as a transient cavity near the next positive pressure peak. This effect is illustrated in Figure 5(a) for ambient pressures of 0.05 and 0.1 MPa. In contrast, for the case with inclusion of the media elastic response, at low ambient pressures, the bubble collapses as a transient cavity during one pressure cycle. Also, all three radius–time curves corresponding to the pressures

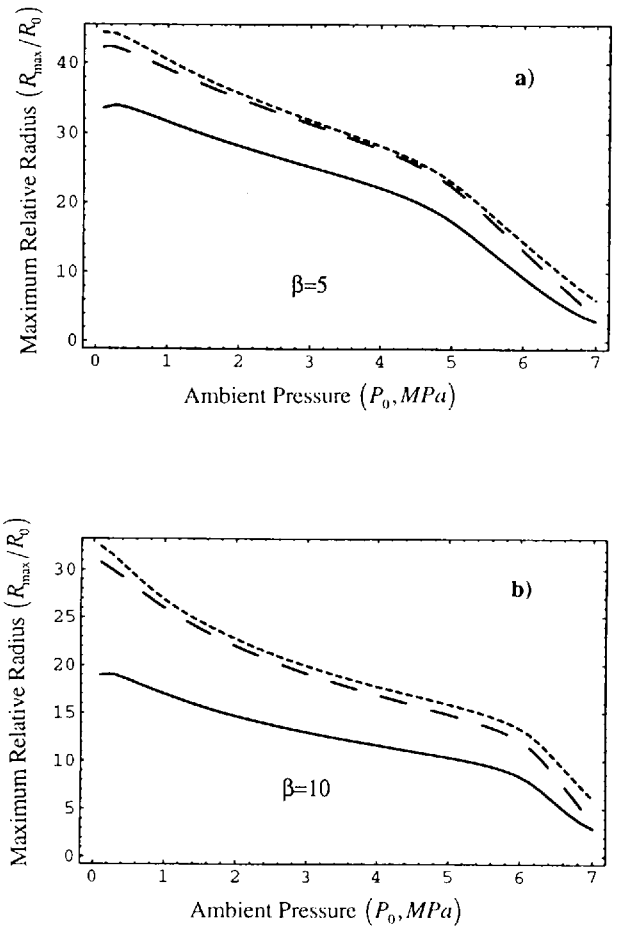

Figure 7 Maximum relative radius of the cavity as a function of ambient pressure for media elastic response (solid line) and for the Notlingk–Neppiras model [dashed and dotted lines correspond to exact solution of eq. (15) and approximation (22)]. f = 20 kHz; A = 31.5 μm; R_0 = 25 μm.

P_0 = 0.05, 0.1, and 0.5 MPa are almost indistinguishable [solid curves on Fig. 5(a)].

Figure 7 summarizes the results of calculation of the maximum cavitation radius as a function of ambient pressure for two different values of parameter β (in MPa^{-1}) which specifies the rate of voids formation. The higher value of β leads to a lower maximum cavitation bubble radius due to the fact that the acoustic pressure amplitude decreases with increasing β. It can be seen that media elastic response has a strong effect on maximum cavitation radius, reducing its value up to 50%.

If one neglects the force due to the surface tension, the following analytical approximation can be derived[33] for the Notlingk–Neppiras model:

$$R_{max} \approx \frac{0.4}{f}\left(1 - \frac{P_0}{P_A}\right)\sqrt{\frac{P_A}{\rho_0}} \qquad (22)$$

For comparison, approximation (22) is also plotted in Figure 7. It can be seen that eq. (22) closely approximates R_{max} derived from the Notlingk–Neppiras model. It should be noted that in the present case the surface tension has very little effect on the cavitation process.

Die Filling Modeling

The flow in a disk die with outer radius R_1 and inner radius R_2 is modeled as a one-dimensional flow in a strip of length $L = R_1 - R_2$ and varying width w. Width variation along the flow direction is calculated as $w(x) = 2\pi(R_1 - x)$. Schematics of this die along with computational flow domain are shown in Figure 8. The simulation of one-dimensional flow in a cavity of simple geometry can be summarized in terms of transport equations. For the case of a strip of width w and half-gap thickness h, these equations are[34,35]:

$$Q = w\int_{-h}^{h} u dz \qquad (23)$$

$$0 = \frac{\partial}{\partial z}\left(\eta\frac{\partial u}{\partial z}\right) - \frac{\partial P_0}{\partial x} \qquad (24)$$

$$\rho_0 c_p \frac{\partial T}{\partial x} = k_{th}\frac{\partial^2 T}{\partial x^2} + \Phi + \dot{Q}_s + \dot{Q}_d \qquad (25)$$

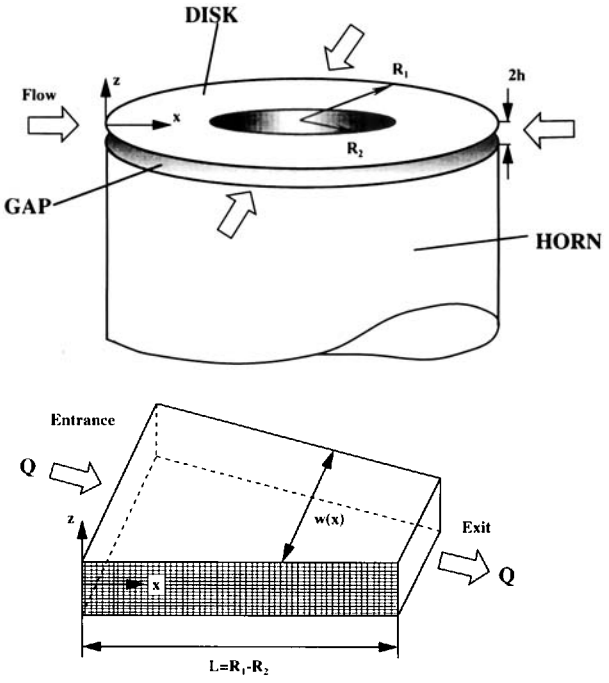

Figure 8 Schematics of the die geometry and computational domain.

where Q denotes the volumetric flow rate; x, the streamwise direction; and z, the gapwise (transverse) direction. Further, u denotes the velocity in the x direction; η, the shear viscosity; P_0, the pressure; and T, the temperature, with c_p and k_{th} denoting specific heat and thermal conductivity, respectively. $\Phi = \eta\dot{\gamma}^2$ and $\dot{Q}_s = 2\pi^2\epsilon^2 f E''$ are rates of viscous and ultrasound dissipation, respectively, where $\dot{\gamma} = |(\partial u)/(\partial z)|$ is the shear rate, $\epsilon = [A/(2h)]$ is the ultrasound strain amplitude, and E'' is the loss modulus at frequency f. $\dot{Q}_d = [(E_C\dot{N}_{C_k} + \sum E_{v_k}\dot{N}_{v_k})/N_A]$ is the rate of energy consumption due to devulcanization. Here, E_C is the energy to rupture a C—C bond, and E_{v_k}, the energy of the scission of k-type crosslinks.

Equation (23) represents a balance of mass, whereas eq. (24) gives the force balance in the streamwise direction between the viscous shear stress and the pressure gradient. Inertial effects have been omitted from the left side of eq. (24) due to the high viscosities typical of polymer melts. Equation (25) is the quasi-stationary energy equation. It indicates that the change in temperature as one follows a material particle is due to the net effect arising from the gapwise thermal conduction, viscous and ultrasound heating, and energy consumption by devulcanization.

Equations (23)–(25) have to be supplemented with a viscosity function as well as boundary conditions. The viscosity is a function of a temperature, shear rate, and gel fraction. This function is represented by a power-law model:

$$\eta = m(T, \xi)\dot{\gamma}^{n-1} \tag{26}$$

The parameters of eq. (26) are based upon fitting experimental data obtained for dependence of viscosity vs. shear rate, temperature, and gel fraction of devulcanized rubber. The following function is used to describe temperature and gel fraction dependence of the viscosity of devulcanized rubber obtained in a wide range of processing conditions:

$$m(T, \xi) = B \exp\left[\frac{b(\xi)}{RT}\right] \tag{27}$$

where B is a constant, and $b(\xi)$, a polynomial function.

For the case of symmetry with respect to plane $z = 0$, the boundary conditions on $u(x, z)$, $T(x, z)$, and $P_0(x)$ are

$$u(x, h) = 0; \quad \frac{\partial u(x, 0)}{\partial z} = 0; \quad 0 \le x \le L \tag{28}$$

$$T(0, z) = T_0; \quad 0 \le z \le h; \quad T(x, h) = T_w;$$

$$0 \le x \le L; \quad \frac{\partial T(x, 0)}{\partial z} = 0; \quad 0 < x \le L \tag{29}$$

$$P_0(L) = P_{atm} \tag{30}$$

where T_0 and T_w are prescribed temperatures at the die entrance and die wall, respectively, and P_{atm} is atmospheric pressure.

The present simulation will be carried out for a constant flow rate. The pressure distribution in the die is an unknown function which has to be calculated using an iterative procedure.

SIMULATION ALGORITHM

The simulation procedure of the flow in the die is simplified by introducing the function $S = \int_0^h (z^2/\eta)\,dz$ which is a measure of the fluidity of the polymer melt. Then, the pressure gradient $\Lambda_x = -[(dP_0)/(dx)]$, velocity u, and shear rate $\dot{\gamma}$ are expressed from eqs. (23) and (24), taking into account the boundary conditions (28). Resulting equations are[34]

$$\Lambda_x = \left(\frac{Q}{2wS}\right)^n; \quad u = \Lambda_x^{1/n}\int_0^h \left[\frac{z}{\eta_0 m(T, \xi)}\right]^{1/n} dz;$$

$$\dot{\gamma} = -\Lambda_x \frac{z}{\eta} \tag{31}$$

The energy eq. (25) is approximated by a finite-difference scheme. For stability reasons, an upwind difference is used to express the streamwise convection term. An implicit representation in the gapwise direction is used for the temperature in the conduction term. Introducing an uniform mesh (x_i, z_j) as

$$x_i = (i - 1)\Delta x, \quad 1 \le i \le N_x$$

$$z_j = (j - 1)\Delta z, \quad 1 \le j \le N_z \tag{32}$$

the finite-difference approximation of the energy eq. (25) in the inner nodes is

$$\rho_0 c_p u_{i,j}\frac{T_{i+1,j} - T_{i,j}}{\Delta x} = k_{th}\frac{T_{i,j+1} - 2T_{i,j} + T_{i,j-1}}{\Delta z^2} + \dot{Q}_{i,j}^{(tot)} \tag{33}$$

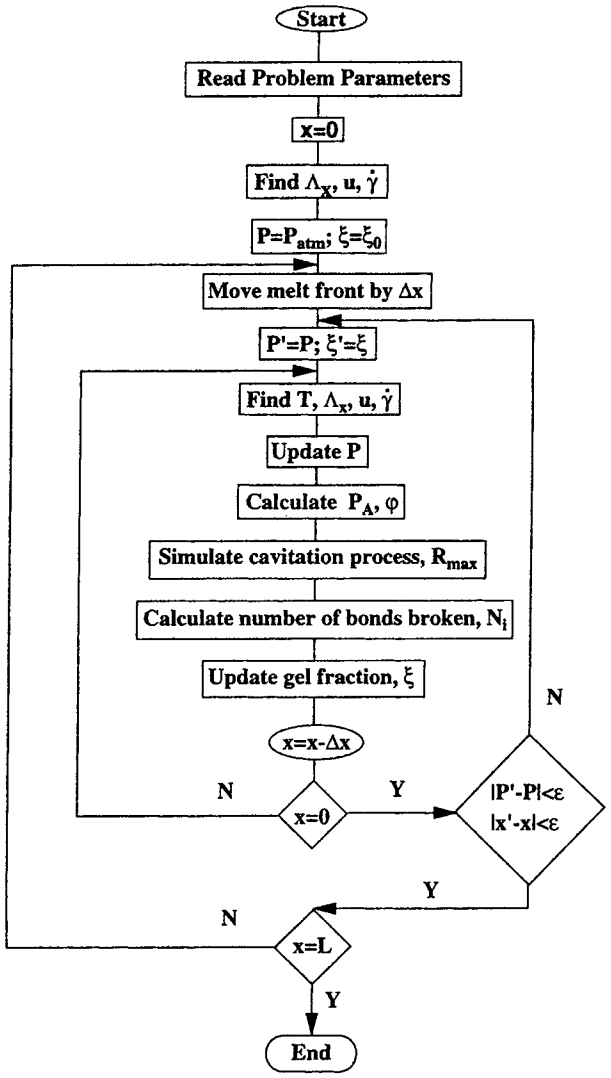

Figure 9 Computational flow chart.

The finite-difference approximations of the temperature boundary conditions (29) with the second-order accuracy are

$$T_{1,j} = T_0; \quad 1 \le j \le N_z$$

$$T_{i,1} = \frac{4}{3}T_{i,2} - \frac{1}{3}T_{i,3}, \quad T_{i,N_z} = T_w;$$

$$1 < i \le N_x \quad (34)$$

In eq. (33), $\dot{Q}_{i,j}^{(tot)}$ is the grid function of the total energy consumption:

$$\dot{Q}_{i,j}^{(tot)} = \Phi(x_i, z_j) + \dot{Q}_s(x_i, z_j) + \dot{Q}_d(x_i, z_j)$$

The simulation algorithm is as follows: When the melt front moves from a position x_i to x_{i+1}, the temperature distribution along the new melt front is initially calculated using the old values of u, $\dot{\gamma}$, and T at x_i. Then, the pressure gradient, velocity, and shear rate are calculated by eq. (31) based upon the updated temperature field. The pressure is determined by numerical quadrature of Λ_x, starting with zero at the melt front and integrating back toward the die entrance. During this procedure, the value of the pressure is updated first. With this updated ambient pressure, P_0, the acoustic pressure amplitude, P_A, is calculated by eq. (21) using the Newton–Raphson method. Then, the number of bubbles per unit volume, N_b, is evaluated from eq. (18). At the same time, the bubble growth and collapse process is simulated and R_{max} is evaluated according to eq. (15). Calculated values of N_b and R_{max} are utilized to determine the number of broken bonds according to eq. (4) and material gel fraction, ξ, and crosslink density, $N_\nu(t)$, according to eqs. (6) and (7). After that, the temperature T, pressure gradient Λ_x, and kinematics characteristics u, $\dot{\gamma}$ are reevaluated using the updated values of the gel fraction and pressure. This cycle is then repeated. The iterative process is continued until a prescribed convergence criterion is satisfied between successive cycles. The calculation is continued until the die is filled. The final distribution of various quantities corresponds to the stationary solution of the devulcanization process. Figure 9 shows the computational flow chart outlined above. The simulation results based on the proposed devulcanization model and computational algorithm will be presented in Part II of this study.

CONCLUSIONS

The present study describes theoretical results related to a novel ultrasonic devulcanization technology for recycling used tires and other rubber waste. A model of the devulcanization process is proposed. The model is based upon the ability of high-intensity ultrasonic waves to introduce cavitation in a vulcanized rubber. In the modeling of the cavitation process, a stress term arising due to elastic deformation of rubber is incorporated into evolution of bubble dynamics. In addition, the dependence of the number of bubbles per unit volume on the difference between acoustic and ambient pressures is introduced into the model. These values along with the value of R_{max} and various bond energies are used to determine the amounts of various broken bonds. This breakup of a three-dimensional network in crosslinked rubbers on a microlevel is combined with flow modeling on a macrolevel using proposed mod-

ification of the power-law rheological equation. The latter incorporates the dependence of viscosity of devulcanized rubber on shear rate, temperature, and gel fraction. A simulation procedure for velocity, temperature, pressure, and structural characteristics such as gel fraction and fractions of various broken bonds is described.

This work was supported by Grant DMI-9312249 from the National Science Foundation, Division of Engineering.

REFERENCES

1. A. I. Isayev, C. M. Wong, and X. Zeng, *SPE ANTEC Tech. Pap.*, **33,** 207 (1987).
2. A. I. Isayev, in *Proceedings of the 23rd Israel Conference of Mechanical Engineering,* 1990, Paper #5.2.3, p. 1.
3. A. I. Isayev, C. M. Wong, and Z. Zeng, *Adv. Polym. Technol.*, **10,** 31 (1990).
4. H. H. G. Jellinek, in *Encyclopedia of Polymer Science and Technology,* H. F. Mark, N. G. Gaylord, and N. M. Bikales, Eds., Wiley-Interscience, New York, 1966, Vol. 4.
5. I. E. El'piner, *Ultrasound: Physical, Chemical and Biological Effects,* Consultants Bureau, New York, 1964.
6. A. Casale and R. S. Porter, *Polymer Stress Reactions,* Academic Press, New York, 1977.
7. K. S. Suslick, *Sci. Am.*, **260,** 80 (1989).
8. K. S. Suslick, S. J. Doktycz, and E. B. Flint, *Ultrasonics,* **28,** 280 (1990).
9. S. L. Peshkovskii, M. L. Friedman, A. I. Tukachinsky, G. V. Vinogradov, and N. S. Enikolopian, *Polym. Compos.*, **4,** 126 (1983).
10. A. I. Isayev and S. Mandelbaum, *Polym. Eng. Sci.*, **31,** 1051 (1991).
11. A. I. Isayev, U.S. Pat. 5,258,413 (1993).
12. A. I. Isayev and J. Chen, U.S. Pat. 5,284,625 (1994).
13. A. I. Isayev, J. Chen, and A. Tukachinsky, *Rubb. Chem. Technol.*, **68,** 267 (1995).
14. A. Tukachinsky, D. Schworm, and A. I. Isayev, to appear.
15. A. I. Isayev, J. Chen, and S. P. Yushanov, in *Advances in Simulation of Industrial Forming Processes,* S. F. Shen and P. Dawson, Eds., Balkema, Rotterdam, 1995.
16. W. C. Warner, *Rubb. Chem. Technol.*, **67,** 559 (1994).
17. L. Treloar, *The Physics of Rubber Elasticity,* 3rd ed., Oxford University Press, London, 1975.
18. A. V. Tobolsky, *Property and Structure of Polymer,* Wiley, New York, 1960.
19. H. G. Flynn, in *Physical Acoustics,* W. P. Mason, Ed., Academic Press, New York, 1964, Vol. I, Part B.
20. F. R. Young, *Cavitation,* McGraw-Hill, London, 1989.
21. A. E. Green and W. Zerna, *Theoretical Elasticity,* Oxford University Press, London, 1954.
22. A. N. Gent and P. B. Lindley, *Proc. R. Soc. Lond. Ser. A,* **249,** 195 (1958).
23. A. N. Gent and A. G. Thomas, *J. Polym. Sci.*, **28,** 623 (1958).
24. B. E. Notlingk and A. E. Neppiras, *Proc. Phys. Soc. B (Lond.)*, **63,** 674 (1950).
25. B. E. Notlingk and A. E. Neppiras, *Proc. Phys. Soc. B (Lond.)*, **64,** 1032 (1951).
26. L. E. Kinsler, A. R. Frey, A. B. Coppens, and J. V. Sanders, *Fundamentals of Acoustics,* Wiley, New York, 1982.
27. M. Minndert, *Philos. Mag.*, **16,** 235 (1933).
28. L. van Wijngaarden, *Annu. Rev. Fluid Mech.*, **4,** 369 (1972).
29. E. L. Castersen and L. L. Foldy, *J. Acoust. Soc. Am.*, **19,** 481 (1947).
30. C. E. Brennen, *Cavitation and Bubble Dynamics,* Oxford University Press, New York, 1995.
31. A. N. Gent and D. A. Tompkins, *J. Appl. Phys.*, **20,** 2520 (1967).
32. V. E. Nokoryakov, B. G. Pokusaev, and I. R. Shreiber, *Wave Propagation in Gas-Liquid Media,* CRS Press, Boca Raton, FL, 1993.
33. B. A. Agranat, V. I. Bashkirov, and Yu. I. Kitaigorodskii, in *Ultrasonic Cleaning, Physical Principles of Ultrasonic Technology,* L. D. Rosenberg, Ed., Plenum Press, New York, 1973, Vol. 1.
34. C. A. Hieber, in *Injection and Compression Molding Fundamentals,* A. I. Isayev, Ed., Marcel Dekker, New York, 1987.
35. A. I. Isayev, Ed., *Modeling of Polymer Processing,* Hanser, Munich, 1991.

Received June 16, 1995
Accepted August 11, 1995